

A New Method for Fitting Current–Voltage Curves of Planar Heterojunction Perovskite Solar Cells

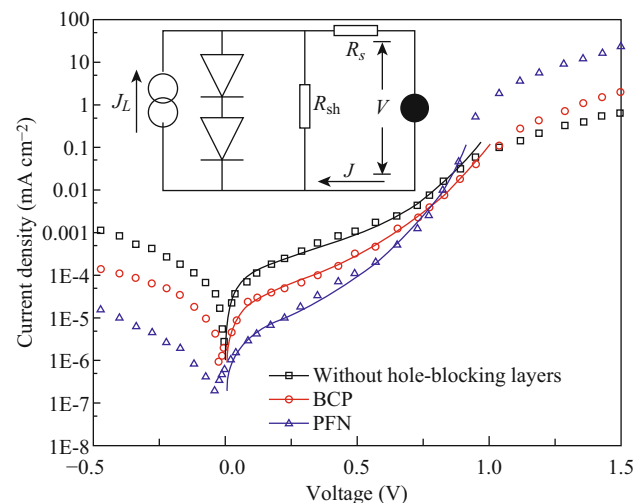
Peizhe Liao¹ · Xiaojuan Zhao¹ · Guolong Li² · Yan Shen¹ · Mingkui Wang¹

Received: 22 July 2017 / Accepted: 11 September 2017 / Published online: 13 October 2017
© The Author(s) 2017. This article is an open access publication

Highlights

- A universal and simple method to analyze current-voltage curves of planar heterojunction perovskite solar cells is proposed.
- The new method theoretically solves the dilemma of the parameter diode ideal factor being larger than 2.
- The dark current fitted with the new method helps to analyze physical processes of perovskite solar cells.

Abstract Herein we propose a new equivalent circuit including double heterojunctions in series to simulate the current-voltage characteristic of P–I–N planar structure perovskite solar cells. This new method can theoretically solve the dilemma of the parameter diode ideal factor being larger than 2 from an ideal single heterojunction equivalent circuit, which usually is in the range from 1 to 2. The diode ideal factor reflects PN junction quality, which influences the recombination at electron transport layer/perovskite and perovskite/hole transport layer interface. Based on the double PN junction equivalent circuit, we can also simulate the dark current–voltage curve for analyzing recombination current (Shockley–Read–Hall recombination) and diffusion current (including direct recombination), and thus carrier recombination and transportation characteristics. This new model offers an efficacious and simple method to investigate interfaces condition, film quality of perovskite absorbing layer and performance of transport layer, helping us further



improve the device efficiency and analyze the working mechanism.

✉ Mingkui Wang
mingkui.wang@mail.hust.edu.cn

¹ Wuhan National Laboratory for Optoelectronics, Huazhong University of Science and Technology, Luoyu Road 1037, Wuhan 430074, People's Republic of China

² Ningxia University, Helan Mountain Road 489, Yinchuan 750021, People's Republic of China

Keywords Dark current · Device simulation · Junction property · Perovskite · Solar cell

1 Introduction

The photoelectric effect converts solar energy into electricity, which is one of the promising ways to solve the global energy crisis and environmental pollution. Due to the excellent light absorption and carrier transportation characteristics, perovskite-type semiconductors with a general ABX_3 formula have attracted intensive interest in recent years [1]. The power conversion efficiency (PCE) of perovskite solar cell (PSC) has a rapid growth from 3.8% in 2009 to 22.1% in 2016 [2, 3]. Despite this, it is important to understand the carrier transport mechanism of PSCs, while it is a good way to fit current–voltage (J – V) curves. Hence the J – V curves for silicon solar cells and thin-film solar cells have been fitted to analyze the working mechanism and performance of solar cells [4–6]. Considering the absence of specific equivalent circuit and fitting formula for P–I–N model, an ideal single PN junction circuit has been built to simulate the J – V characteristic of various PSCs [7]. By fitting J – V curves under light and in dark, three parameters including series resistance (R_s), diode ideal factor (m) and reverse saturation current (J_0) can be obtained. Compared to the reverse saturation current of conventional semiconductor diodes (such as CdTe, GIGS), the parameter J_0 of PSC is relatively low, which explains its smaller bandgap voltage loss (~ 0.4 eV) [8]. Therefore, it is helpful to improve the efficiency of PSC by understanding the two parameters of R_s and J_0 [9]. Furthermore, the parameter m has been utilized as an indication of the heterojunction solar cell [7].

To date, planar-structured PSCs have been developing rapidly due to their various advantages of simple device structure, low-temperature processable fabrication and so on [10]. Nevertheless, in planar PSCs, the value of m obtained by single PN junction modeling does not fill in the theoretical expectation, indicating that the heterojunction property in planar PSCs further discussion [11, 12]. Generally, for a single heterojunction model, the ideal factor approaches to 1 when the carrier diffusion in the neutral region of semiconductors dominates the diode current through a PN junction. On the other hand, the ideal factor

approaches to 2 when the diode current is dominated by carrier indirect recombination in depleted space-charge region [9]. Theoretically, the smaller value of m reflects the less carrier recombination induced by the interface defect state. In most cases, both diffusion and composite currents exist simultaneously, and therefore, the parameter m is in the range of 1–2. Interestingly, we note that, as shown in Table 1, most of the calculation results are larger than 2. Hence a single PN junction model (Fig. 1a) is not suitable to planar heterojunction PSCs [13, 14].

In this work, we present a new equivalent circuit to investigate the heterojunction property for planar PSCs (in light and dark). Based on the new double heterojunction circuit, we found that smaller value of m reflects better PN junction quality in PSCs. Moreover, carrier recombination and transportation characteristics can be further explored by fitting J – V curve in dark with the new model for describing these important processes in efficient PSC devices.

2 Theoretical Background

Firstly, the rectification characteristic of heterojunction solar cell can be typically described by the Shockley diode equation (Eq. 1) [14],

$$J_D = J_0 \left\{ e^{\frac{qV}{mKT}} - 1 \right\} \quad (1)$$

where J_D is the dark current, V is the applied voltage, J_0 is the reverse saturation current density, q is the elementary charge, m is the ideal factor of a heterojunction, K is the Boltzmann constant, T is the absolute temperature. Under the ideal condition of sunlight, photocurrent can be added into Eq. 1:

$$J = J_{ph} - J_0 \left\{ e^{\frac{qV}{mKT}} - 1 \right\} \quad (2)$$

where J_{ph} is the photocurrent. In fact, output current (J) in Eq. 2 is limited by internal resistance and leakage current in PSCs. Figure 1a presents ideal circuit model with a single PN junction, from which the J – V curve (in light) of

Table 1 Calculated ideal factor (m) on planar heterojunction PSCs based on single PN junction model reported in the literatures

| Device architecture | Ideal factor (m) | References |
|--|----------------------|------------|
| ITO/PEDOT:PSS/CH ₃ NH ₃ PbI _{3-x} Cl _x /PCBM/PFN/Al | 2.3 | [16] |
| FTO/CH ₃ NH ₃ PbI _{3-x} Cl _x /Spiro-OMeTAD/Au | 3.39 | [38] |
| Mg-ZnO/CH ₃ NH ₃ PbI _{3-x} Cl _x /Spiro-OMeTAD/Au | 2.6–3.0 | [39] |
| ITO/PEDOT:PSS/Perovskite/PCBM/BCP/Ag | 2.2 | [40] |
| ITO/PEDOT:PSS/CH ₃ NH ₃ PbI ₃ /C ₆₀ /Al | 3.51 | [41] |
| FTO/Mg-TiO ₂ /Perovskite/Spiro-OMeTAD/Au | 2.1 | [42] |
| FTO/TiO ₂ /C ₆₀ /(FA) _x (MA) _{1-x} PbI ₃ /Spiro-OMeTAD/Au | 2.6–2.92 | [43] |

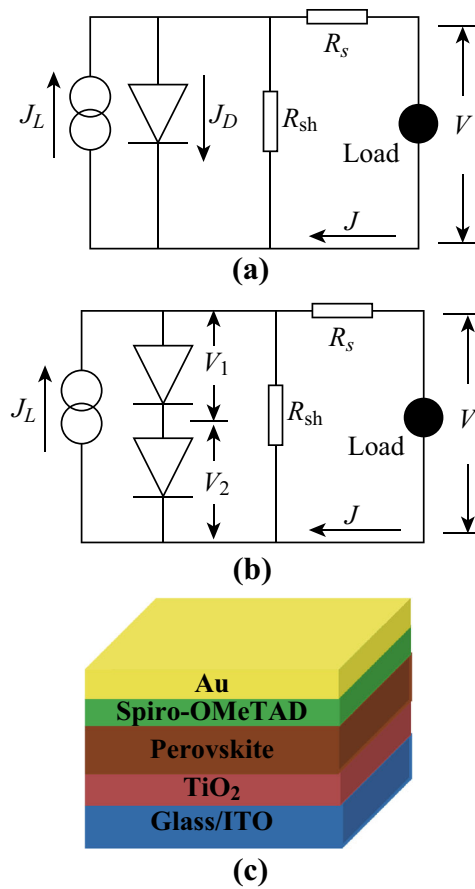


Fig. 1 **a** Single PN junction model for PSCs and **b** new double PN junction model improved for planar perovskite solar cells with J_L (the light induced current), J_D (the dark current or the forward current of PN junction diode under the sunlight), R_s (the series resistance), R_{sh} (shunt resistance, a fictional parameter to represent the size of leakage current), J (output current of the cell) and V (voltage flowing through the external load). **c** Planar heterojunction perovskite solar cells with $\text{TiO}_2/\text{CH}_3\text{NH}_3\text{PbI}_{3-x}\text{Cl}_x/\text{Spiro-OMeTAD}/\text{Au}$ device architecture. (Color figure online)

heterojunction PSC can be further described with Eq. 3 [15],

$$J = J_{ph} - J_0 \left\{ e^{\frac{q(V+JR_s)}{mKT}} - 1 \right\} - \frac{V + JR_s}{R_{sh}} \quad (3)$$

where R_s and R_{sh} are the series and shunt resistance, respectively. Under the circumstances, R_s , R_{sh} , J_0 and m can be numerically obtained by simulation the J - V curves (both in light and dark) of PSCs with Eq. 3. The R_s reflects the internal resistance, and R_{sh} is a fiction parameter to represent the leakage current. The value of J_0 is directly related to the recombination rate, indicating the thermal emission rate of electrons from the valence band to the conduction band in light absorption layer [16], which also has an impact on the open-circuit voltage. Nevertheless, compared with R_s and J_0 , m , correlating with Shockley–

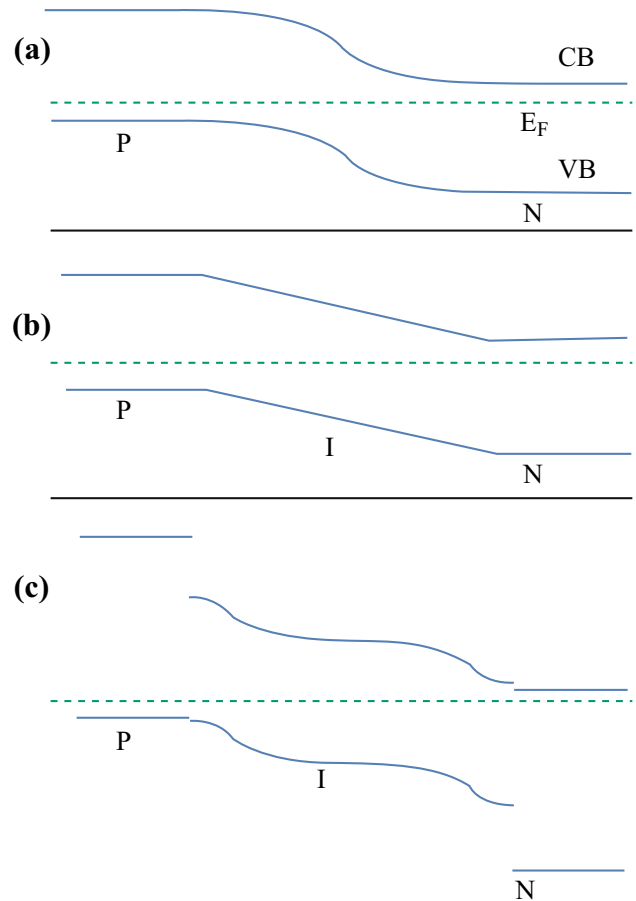


Fig. 2 Energy band diagram of different PN junction photovoltaic devices. **a** A PN junction solar cell. **b** A P–I–N solar cell with homogeneous built-in electric field. **c** $\text{CH}_3\text{NH}_3\text{PbI}_{3-x}\text{Cl}_x$ perovskite-based cell with inhomogeneous built-in electric field. (Color figure online)

Read–Hall recombination [6], is a rarely discussed parameter in PSCs when fitting J - V curves with using single PN junction model [17–20].

Compared to traditional P–I–N structure solar cells (‘a-Si: H’-like), inhomogeneous built-in field of PSCs results in different band structure (Fig. 2) [21, 22]. When the perovskite light absorption layer is sandwiched between n- and p-type charge selective contacts (Fig. 1c), two active junctions immediately form at the n-type electron transport layer (ETL) and the p-type hole transport layer (HTL) sides [22]. Therefore, we suggest two PN junctions in series for explaining planar heterojunction PSCs [23–27], rather than a single PN junction. Equation 4 is applied according to the equivalent circuit of double PN junction as shown in Fig. 1b:

$$V_1 + V_2 = V + JR_s \quad (4)$$

According to the characteristics of the series circuit, the current through the double PN junction should be identical (Eq. 5).

$$J_{01} \left\{ e^{\frac{qV_1}{m_1 kT}} - 1 \right\} = J_{02} \left\{ e^{\frac{qV_2}{m_2 kT}} - 1 \right\} \tag{5}$$

where $m_1, V_1, J_{01}, m_2, V_2, J_{02}$ are diode ideality factor, voltage and reverse saturation current of ETL/perovskite and perovskite/HTL two PN junctions, respectively.

In this study, perovskite absorption layer acts as intrinsic semiconductor, which is fully depleted with highly doped P/N selective layers to form versatile PIN photovoltaics [28]. Considering the condition of $J_{01} \propto P_n D_p / L_p, J_{02} \propto N_p D_n / L_n$ and a similar carrier density for electrons and holes [29, 30], the value of D_p / L_p can be approximately equal to D_n / L_n [31]. Therefore, the difference of the calculated J_{01} and J_{02} values lies in the same magnitude in this case according to the derivation process (Eq. 6).

$$J_{01} \cong J_{02} = J_0 \tag{6}$$

Then Eq. 3 can be further revised as Eq. 7:

$$J = J_{ph} - J_{01} \left\{ e^{\frac{qV_1}{m_1 kT}} - 1 \right\} - \frac{V + JR_s}{R_{sh}} \tag{7}$$

According to Eqs. 4–7, Eq. 8 and Eq. 9 can be inferred:

$$J = J_L - J_0 \left\{ e^{\frac{q(V+JR_s)}{(m_1+m_2)kT}} - 1 \right\} - \frac{V + JR_s}{R_{sh}} \tag{8}$$

$$\frac{V_1}{m_1} = \frac{V_2}{m_2} = \frac{V + JR_s}{m_1 + m_2} \tag{9}$$

Equation 8 describes the J – V curve of planar PSCs under illumination. Since m in Eq. 3 includes the contribution from the double junctions, the sum of m_1 and m_2 can be in the range of 2–4. In short, the calculation results of m (~ 2 –4) in Table 1 confirm the suitability of the proposed double heterojunction equivalent circuit for the planar PSC devices, with which carrier transportation (including direct recombination) and recombination (Shockley–Read–Hall recombination) processes can be precisely described.

3 Results and Discussion

In order to elucidate the effect of m on planar PSCs, we fabricated $\text{CH}_3\text{NH}_3\text{PbI}_3$ -based planar PSC devices with structure of $\text{ITO}/\text{TiO}_2/\text{CH}_3\text{NH}_3\text{PbI}_{3-x}\text{Cl}_x/\text{Spiro-OMeTAD}/\text{Au}$ using two-step deposition method [23], in which methylammonium chloride (MACl) was added to increase the perovskite films quality. Figure 3a shows the typical J – V characteristics of these devices under simulated sunlight at 100 mW cm^{-2} (AM 1.5G). Table 2 shows the photovoltaic parameters of devices with perovskite layers by varying MAcl concentration.

The addition of Cl^- in the perovskite film significantly improved the efficiency of planar PSCs. The maximum performance was obtained for doping the appropriate

amount of MAcl (MAI:MAcl = 50:5), which resulted in highly efficient devices exhibiting short-circuit current (J_{sc}) of 20.35 mA cm^{-2} , open-circuit voltage (V_{oc}) of 1.05 V, fill factor (FF) of 72.73%, corresponding to PCE of 15.6%. The keys to improve the performance of $\text{CH}_3\text{NH}_3\text{PbI}_{3-x}\text{Cl}_x$ devices were better crystallinity of perovskite film, pin hole-free coverage of the perovskite films and fewer interface defect states [32, 33].

We further fitted these J – V curves of devices in Fig. 3a to investigate the effect of doping Cl on perovskite layers by analyzing the parameters of $R_{sh}, R_s, m_1 + m_2$ and J_0 . R_{sh} can be calculated from the inverse of the slope of the J – V curves at 0 V [34]. The other three parameters ($R_s, m_1 + m_2, J_0$) can be obtained through deduction of Eq. 8 as follows,

$$-\frac{dV}{dJ} = \frac{(m_1 + m_2)KT}{q} \left(\frac{1 + R_{sh}^{-1} \frac{dV}{dJ}}{J_{sc} - J - V/R_{sh}} \right) + R_s \tag{10}$$

$$\ln(J_{sc} - J - V/R_{sh}) = \frac{q}{(m_1 + m_2)KT} (V + JR_s) + \ln J_0 \tag{11}$$

R_s can be obtained by calculating the intercept of fitting curve of $-dV/dJ$ versus $\left(\frac{1 + R_{sh}^{-1} \frac{dV}{dJ}}{J_{sc} - J - V/R_{sh}} \right)$ (Eq. 10) in Fig. 3b. Similarly, J_0 can be obtained by fitting the curve of $\ln(J_{sc} - J - V/R_{sh})$ versus $(V + JR_s)$ (Eq. 11) in Fig. 3c. The value of $(m_1 + m_2)$ can be simultaneously inferred from the slope of fitting curves (Eq. 11) in Fig. 3c. The calculation results of four parameters ($R_{sh}, R_s, m_1 + m_2, J_0$) are shown in Table 3.

As shown in Table 3, the shunt resistance R_{sh} dramatically increases from 840 to 5050, 4280, and 3400 Ω for addition of Cl ions (MAI:MAcl from 50:0 to 50:7.5) in perovskite films. A larger R_{sh} indicates less leakage current. This could be related to less pinholes for perovskite layers with Cl^- than that without additives [32, 35]. It is significant that the ideal factor ($m_1 + m_2$) drastically decreases from 3.27 to 2.66 after adding Cl^- and then keeps similar value of 2.66. The value of ideal factor ($m_1 + m_2$) is 3.27, 3.07, 2.66, and 2.64 for corresponding devices, respectively, which further conforms the feasibility of the double PN junction model. Smaller value of $m_1 + m_2$ indicates better PN junction quality [6]. The reverse saturation current (J_0) of corresponding devices was estimated to be $1.69 \times 10^{-4}, 8.23 \times 10^{-5}, 6.89 \times 10^{-6}$ and $4.10 \times 10^{-6} \text{ mA cm}^{-2}$. The smaller J_0 is a sign of substantially suppression of the thermal emission rate of electrons from the VB to the CB [16], resulting in higher output voltage. This is verified with the V_{oc} (being 1.05 V) of device with the suitable addition of Cl ions (MAI:MAcl = 50:5) in perovskite layer, which is higher than devices without Cl. In short, the calculated R_{sh} ,

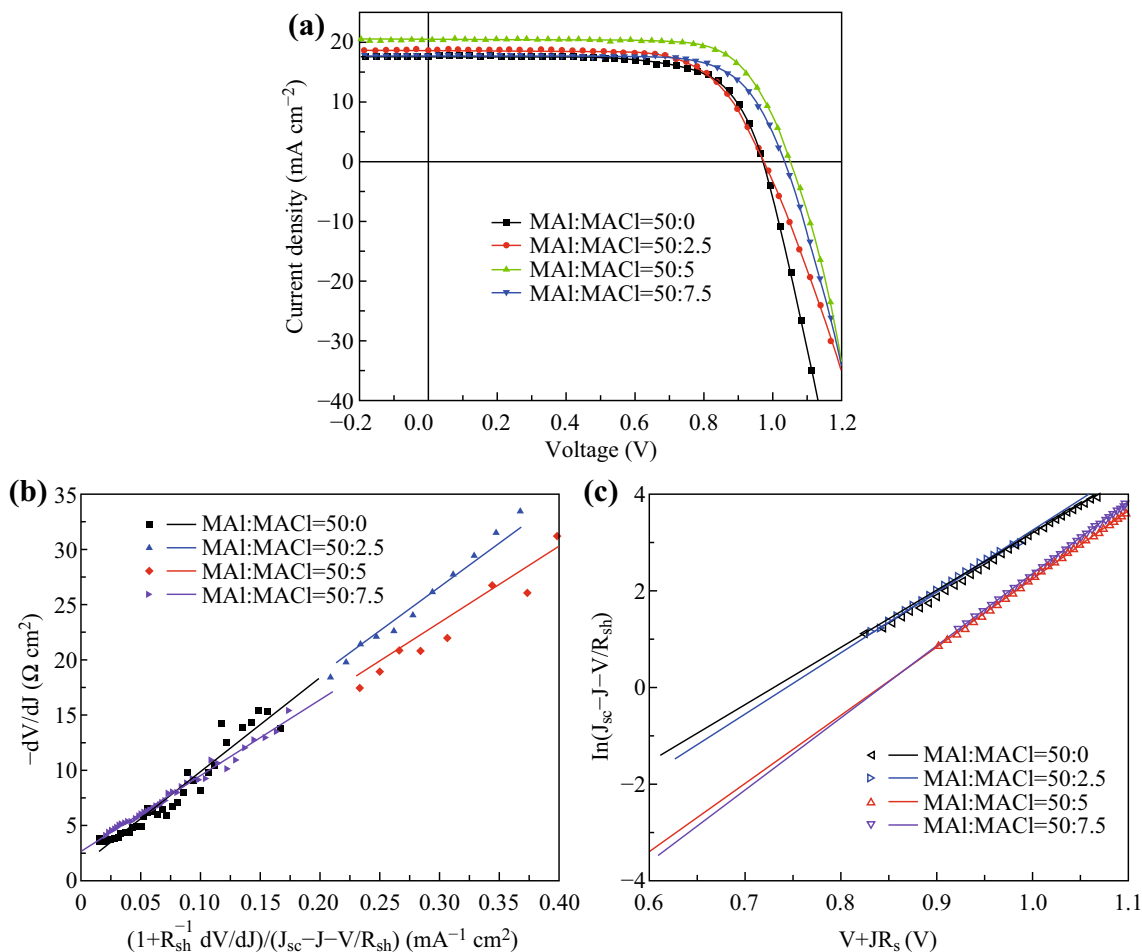


Fig. 3 **a** Current–voltage curve for planar perovskite solar cells using TiO₂/CH₃NH₃PbI_{3-x}Cl_x/Spiro-OMeTAD/Au architecture, the perovskite films prepared by mixing with different concentrations of Cl ions. The measurements are carried out under 100 mW cm⁻². **b** Plots of $-dV/dJ$ versus $\left(\frac{1+R_{sh}^{-1}dV/dJ}{J_{sc}-J-V/R_{sh}}\right)$ (symbols) and the linear fitted curve (solid lines). **c** Plots of $\ln(J_{sc}-J-V/R_{sh})$ versus $V+JR_s$ (symbols) and the linear fitted curve (solid lines). (Color figure online)

Table 2 Photovoltaic performance of perovskite solar cells fabricated from doping varied MACl concentration

| MAI:MACl | J_{sc} (mA cm ⁻²) | V_{oc} (V) | FF (%) | PCE (%) |
|----------|---------------------------------|--------------|--------|---------|
| 50:0 | 17.81 | 0.96 | 68.87 | 11.8 |
| 50:2.5 | 18.64 | 0.98 | 68.75 | 12.5 |
| 50:5 | 20.35 | 1.05 | 72.73 | 15.6 |
| 50:7.5 | 17.54 | 1.03 | 73.53 | 13.3 |

$m_1 + m_2$ further indicates that larger short-circuit current (20.35 mA cm⁻²) for the device with Cl can be attributed to less carrier recombination and loss in ETL/perovskite and perovskite/HTL interfaces.

The dark current was fitted with Eq. 3 (single PN junction model); however, very limited information can be obtained except of three parameters (m , J_0 , R_s) [7]. Furthermore, in the exponential coordinates, the dark current

Table 3 R_{sh} , R_s , $m_1 + m_2$ and J_0 derived from Fig. 3b, c

| MAI:MACl | R_{sh} (Ω cm ²) | R_s (Ω cm ²) | $m_1 + m_2$ | J_0 (mA cm ⁻²) |
|----------|-------------------------------|----------------------------|-------------|------------------------------|
| 50:0 | 840 | 1.41 | 3.27 | 1.69×10^{-4} |
| 50:2.5 | 5050 | 2.72 | 3.07 | 8.23×10^{-5} |
| 50:5 | 4280 | 2.61 | 2.66 | 6.89×10^{-6} |
| 50:7.5 | 3400 | 2.71 | 2.64 | 4.10×10^{-6} |

curve slope varies with the increase in voltage, reflecting different physical processes. This physical process cannot be reflected by Eq. 3 (single PN junction model). In fact, as shown in Fig. 4a, regions A, B, C of dark current is related to shunt current, recombination current and diffusion current, respectively. At last, above the built-in potential at about 1.2 V in region D, the effect of the recombination current is negligible, and the curve is determined only by the diffusion current, limited by the series resistance (R_s) of

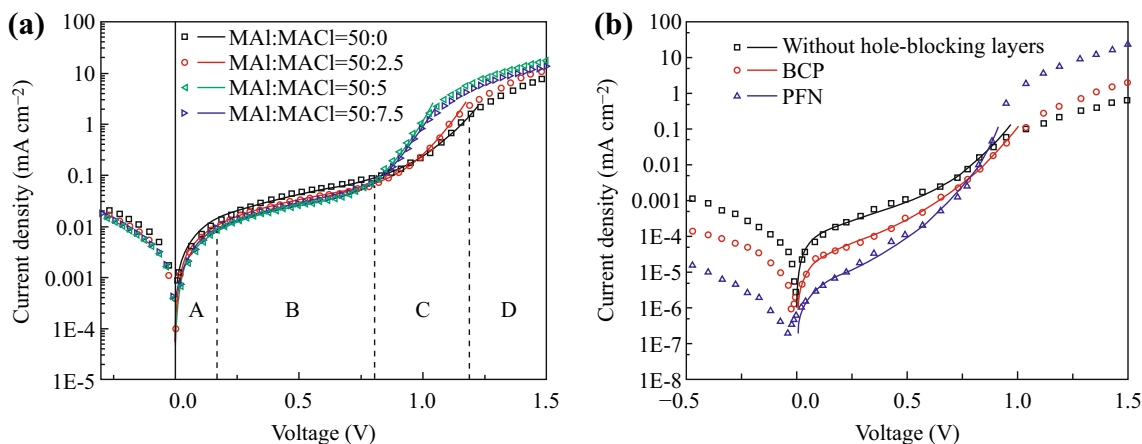


Fig. 4 Plots of dark current of planar PSCs as well as fitting curve by using Eq. 13. **a** The device structure is shown in Fig. 1c, the perovskite films prepared by mixing with different concentrations of Cl ions. **b** The device structure is PEDOT:PSS/CH₃NH₃PbI_{3-x}Cl_x/PCBM/hole-blocking layer/Al, with the original data coming from the Ref. [8]. The inset regions A, B, C, D are mainly determined by shunt current, recombination current in diode space-charge region, diffusion current, diode diffusion current limited by series resistance, respectively. (Color figure online)

Table 4 R_{sh} , J_r , J_d values derived from fitting dark current in Fig. 4a by using Eq. 14

| MAI:MACl | R_{sh} (MΩ cm ²) | J_r (mA cm ⁻²) | J_d (mA cm ⁻²) |
|----------|--------------------------------|------------------------------|------------------------------|
| 50:0 | 12 | 1×10^{-5} | 5×10^{-11} |
| 50:2.5 | 16 | 9×10^{-6} | 3×10^{-10} |
| 50:5 | 20 | 8×10^{-6} | 5×10^{-9} |
| 50:7.5 | 19 | 8×10^{-6} | 3×10^{-9} |

the cell [14]. In order to more accurate quantitative analysis of the dark J - V characteristic in regions A, B, C in the perovskite solar cells, regardless of region D, Eq. 8 can be further deduced in dark (not consider J_L , R_s):

$$J = \frac{V}{R_{sh}} + J_0 \left\{ e^{\frac{qV}{(m_1+m_2)kT}} - 1 \right\} \tag{12}$$

In region A of Fig. 4a, the dark current is mainly affected by the shunt current under the small applied bias voltage. With the bias voltage increase, recombination current is much larger than diffusion current in dark J - V characteristics of planar PSCs, as shown in region B of Fig. 4a. The slope of region B is less than slope of region C, and the steep increment of the current results from a diffusion-dominated current [14]. The dark current-voltage characteristic is in a single exponential relationship in region B and region C, respectively.

Table 5 R_{sh} , J_r , J_d derived from fitting dark current of inverted planar PSCs in Fig. 4b

| Hole-blocking layer | R_{sh} (MΩ cm ²) | J_r (mA cm ⁻²) | J_d (mA cm ⁻²) |
|---------------------|--------------------------------|------------------------------|------------------------------|
| Without | 1 | 3×10^{-6} | 8×10^{-10} |
| BCP | 5 | 1.5×10^{-6} | 4×10^{-10} |
| PFN | 35 | 5×10^{-7} | 1×10^{-9} |

In order to quantitative calculate diffusion current and recombination current, respectively, Eq. 12 is further rewritten by taking into account the heterojunction diffusion model [29, 30]:

$$J = \frac{V}{R_{sh}} + J_r \left\{ e^{\frac{eV_1}{m_{1r}kT}} - 1 \right\} + J_d \left\{ e^{\frac{eV_1}{m_{1d}kT}} - 1 \right\} \tag{13}$$

In Eq. 13, the first term is the shunt current corresponding to region A in Fig. 4a. The second term is the recombination current (Shockley-Read-Hall recombination), $m_{1r} = 2$. The third term is the diffusion current (including carrier directly recombination), $m_{1d} = 1$ [14, 36, 37]. According to Eqs. 9, 13 can be furtherly derived:

$$J = \frac{V}{R_{sh}} + J_r \left\{ e^{\frac{eV}{m_r kT}} - 1 \right\} + J_d \left\{ e^{\frac{eV}{m_d kT}} - 1 \right\} \tag{14}$$

In Eq. 14, $m_r = m_{1r} + m_{2r} = 4$, $m_d = m_{1d} + m_{2d} = 2$. The dark current in Fig. 4a can be fitted by Eq. 14. The calculation results of three parameters (R_{sh} , J_r , J_d) are shown in Table 4.

We fit the dark current of inverted planar heterojunction PSCs in other literatures in order to further verify the formula based on double PN junction equivalent circuit (Fig. 1b) [8].

As shown in Table 5, the parameter R_{sh} of inverted planar PSCs with different hole-blocking layers is 1, 5, and 35 MΩ cm². The recombination current (J_r) of

corresponding devices is 3×10^{-6} , 1.5×10^{-6} , and 5×10^{-7} mA cm⁻². Both of them indicate that hole-blocking layer blocks hole injection into the diode, effectively reducing the shunt current and recombination current. Compared to the BCP, the device with PFN shows better hole-blocking property. The same conclusion obtained by comparing the dark current at -100 mV as discussed in the literatures. Meanwhile, the devices without hole-blocking layer showed larger dark current under reverse bias, mainly due to the larger hole injection into the diode [8]. Moreover, the PFN enhanced electron injection and extraction, which can be verified by drastically increased diffusion current J_d (from 8×10^{-10} to 1×10^{-9} mA cm⁻²). This conclusion confirms the speculation in the literature: PFN improves the electron injection and extraction in PSC devices [8]. Therefore, the new model proposed in this study can be universal and effective to analyze carrier recombination and transportation.

4 Conclusion

In conclusion, we built up a double PN junction equivalent circuit to fit J - V curves of P-I-N planar structure heterojunction PSCs. The new method focuses on the relationship between the diode ideal factor and the carrier recombination from the interface defects. By varying Cl⁻ content in the CH₃NH₃PbI₃ perovskite film, we found that the value of m drastically diminished (decreased) with the perovskite film quality improvement. In order to quantitatively analyze the correlation mechanism of dark current under different bias voltages, a new equation based on the double PN junction equivalent circuit has been proposed to analyze the dark current-voltage curve. Consequently, carrier recombination and loss reduction could be reflected in R_{sh} and J_r . The carrier transmission could be reflected on the parameter J_d . Based on the double PN junction equivalent circuit, the J - V curve in light and in dark could be fitted, respectively, helping us analyze the working mechanism and improve the efficiency of planar PSCs.

Acknowledgements Financial support from the 973 Program of China (No. 2014CB643506 and 2013CB922104), the China Scholarship Council (No. 201506165038), the Natural Science Foundation of China (No. 21673091), the Natural Science Foundation of Hubei Province (No. ZRZ2015000203), Technology Creative Project of Excellent Middle and Young Team of Hubei Province (No. T201511) and the Wuhan National High Magnetic Field Center (2015KF18) is acknowledged.

Open Access This article is distributed under the terms of the Creative Commons Attribution 4.0 International License (<http://creativecommons.org/licenses/by/4.0/>), which permits unrestricted use, distribution, and reproduction in any medium, provided you give appropriate credit to the original author(s) and the source, provide a link to the Creative Commons license, and indicate if changes were made.

References

1. C.R. Kagan, D.B. Mitzi, C.D. Dimitrakopoulos, Organic-inorganic hybrid materials as semiconducting channels in thin-film field-effect transistors. *Science* **286**(5441), 945–947 (1999). doi:[10.1126/science.286.5441.945](https://doi.org/10.1126/science.286.5441.945)
2. H.S. Kim, C.R. Lee, J.H. Im, K.B. Lee, T. Moehl et al., Lead iodide perovskite sensitized all-solid-state submicron thin film mesoscopic solar cell with efficiency exceeding 9%. *Sci. Rep.* **2**(8), 591 (2012). doi:[10.1038/srep00591](https://doi.org/10.1038/srep00591)
3. J. Burschka, N. Pellet, S.J. Moon, R. Humphry-Baker, P. Gao, M.K. Nazeeruddin, M. Gratzel, Sequential deposition as a route to high-performance perovskite-sensitized solar cells. *Nature* **499**(7458), 316–319 (2013). doi:[10.1038/nature12340](https://doi.org/10.1038/nature12340)
4. F. Khan, S.N. Singh, M. Husain, Determination of diode parameters of a silicon solar cell from variation of slopes of the I-V curve at open circuit and short circuit conditions with the intensity of illumination. *Semicond. Sci. Tech.* **25**(1), 015002 (2010). doi:[10.1088/0268-1242/25/1/015002](https://doi.org/10.1088/0268-1242/25/1/015002)
5. S.S. Hegedus, W.N. Shafarman, Thin-film solar cells: device measurements and analysis. *Prog. Photovoltaics* **12**(2–3), 155–176 (2004). doi:[10.1002/ppv.518](https://doi.org/10.1002/ppv.518)
6. J. Kim, J.H. Yun, H. Kim, Y. Cho, H.H. Park, M.M.D. Kumar, J. Yi, W.A. Anderson, D.W. Kim, Transparent conductor-embedding nanocones for selective emitters: optical and electrical improvements of Si solar cells. *Sci. Rep.* **5**(1), 9256 (2015). doi:[10.1038/srep09256](https://doi.org/10.1038/srep09256)
7. J.J. Shi, J. Dong, S.T. Lv, Y.Z. Xu, L.F. Zhu et al., Hole-conductor-free perovskite organic lead iodide heterojunction thin-film solar cells: high efficiency and junction property. *Appl. Phys. Lett.* **104**(6), 063901 (2014). doi:[10.1063/1.4864638](https://doi.org/10.1063/1.4864638)
8. L.T. Dou, Y. Yang, J.B. You, Z.R. Hong, W.H. Chang, G. Li, Y. Yang, Solution-processed hybrid perovskite photodetectors with high detectivity. *Nat. Commun.* **5**, 5404 (2014). doi:[10.1038/ncomms6404](https://doi.org/10.1038/ncomms6404)
9. Y. Li, Z. Xu, S.L. Zhao, B. Qiao, D. Huang et al., Highly efficient P-I-N perovskite solar cells utilizing novel low-temperature solution-processed hole transport materials with linear pi-conjugated structure. *Small* **12**(35), 4902–4908 (2016). doi:[10.1002/sml.201601603](https://doi.org/10.1002/sml.201601603)
10. L. Meng, J.B. You, T.F. Guo, Y. Yang, Recent advances in the inverted planar structure of perovskite solar cells. *Accounts Chem. Res.* **49**(1), 155–165 (2016). doi:[10.1021/acs.accounts.5b00404](https://doi.org/10.1021/acs.accounts.5b00404)
11. Z. Zhou, J. Xu, L. Xiao, J. Chen, Z.A. Tan, J.X. Yao, S.Y. Dai, Efficient planar perovskite solar cells prepared via a low-pressure vapor-assisted solution process with fullerene/TiO₂ as an electron collection bilayer. *RSC Adv.* **6**(82), 78585–78594 (2016). doi:[10.1039/C6RA14372E](https://doi.org/10.1039/C6RA14372E)
12. D. Liu, C. Liu, L.L. Wu, W. Li, F. Chen, B.Q. Xiao, J.Q. Zhang, L.H. Feng, Highly reproducible perovskite solar cells with excellent CH₃NH₃PbI_{3-x}Cl_x film morphology fabricated via high precursor concentration. *RSC Adv.* **6**(56), 51279–51285 (2016). doi:[10.1039/C6RA07359J](https://doi.org/10.1039/C6RA07359J)
13. M.K. Wang, W.L. Yim, P.Z. Liao, Y. Shen, Temperature dependent characteristics of perovskite solar cells. *ChemistrySelect* **2**(16), 4469–4477 (2017). doi:[10.1002/slct.201700776](https://doi.org/10.1002/slct.201700776)
14. G.J.A.H. Wetzelaer, M. Scheepers, A.M. Sempere, C. Momblona, J. Avila, H.J. Bolink, Trap-assisted non-radiative recombination in organic-inorganic perovskite solar cells. *Adv. Mater.* **27**(11), 1837–1841 (2015). doi:[10.1002/adma.201405372](https://doi.org/10.1002/adma.201405372)
15. J.F. Lu, J. Bai, X.B. Xu, Z.H. Li, K. Cao, J. Cui, M.K. Wang, Alternate redox electrolytes in dye-sensitized solar cells. *Chin. Sci. Bull.* **57**(32), 4131–4142 (2012). doi:[10.1007/s11434-012-5409-3](https://doi.org/10.1007/s11434-012-5409-3)

16. J.B. You, Y.M. Yang, Z.R. Hong, T.B. Song, L. Meng et al., Moisture assisted perovskite film growth for high performance solar cells. *Appl. Phys. Lett.* **105**(18), 183902 (2014). doi:[10.1063/1.4901510](https://doi.org/10.1063/1.4901510)
17. W.D. Zhu, C.X. Bao, Y. Wang, F.M. Li, X.X. Zhou et al., Coarsening of one-step deposited organolead triiodide perovskite films via Ostwald ripening for high efficiency planar-heterojunction solar cells. *Dalton Trans.* **45**(18), 7856–7865 (2016). doi:[10.1039/C6DT00900J](https://doi.org/10.1039/C6DT00900J)
18. X.D. Li, X.H. Liu, X.Y. Wang, L.X. Zhao, T.G. Jiu, J.F. Fang, Polyelectrolyte based hole-transporting materials for high performance solution processed planar perovskite solar cells. *J. Mater. Chem. A* **3**(29), 15024–15029 (2015). doi:[10.1039/C5TA04712A](https://doi.org/10.1039/C5TA04712A)
19. E.Z. Li, Y. Guo, T. Liu, W. Hu, N. Wang, H.C. He, H. Lin, Preheating-assisted deposition of solution-processed perovskite layer for an efficiency-improved inverted planar composite heterojunction solar cell. *RSC Adv.* **6**(37), 30978–30985 (2016). doi:[10.1039/C5RA27434F](https://doi.org/10.1039/C5RA27434F)
20. S. Yuan, Z.W. Qiu, H.L. Zhang, H.B. Gong, Y.F. Hao, B.Q. Cao, Oxygen influencing the photocarriers lifetime of $\text{CH}_3\text{NH}_3\text{PbI}_{3-x}\text{Cl}_x$ film grown by two-step interdiffusion method and its photovoltaic performance. *Appl. Phys. Lett.* **108**(3), 033904 (2016). doi:[10.1063/1.4940368](https://doi.org/10.1063/1.4940368)
21. J. Nelson, *The Physics of Solar Cells* (Imperial College Press, London, 2003)
22. E. Edri, S. Kirmayer, S. Mukhopadhyay, K. Gartsman, G. Hodes, D. Cahen, Elucidating the charge carrier separation and working mechanism of $\text{CH}_3\text{NH}_3\text{PbI}_{3-x}\text{Cl}_x$ perovskite solar cells. *Nat. Commun.* **5**, 3461 (2014). doi:[10.1038/ncomms4461](https://doi.org/10.1038/ncomms4461)
23. X.X. Shai, L.J. Zuo, P.Y. Sun, P.Z. Liao, W.C. Huang et al., Efficient planar perovskite solar cells using halide Sr-substituted Pb perovskite. *Nano Energy* **36**, 213–222 (2017). doi:[10.1016/j.nanoen.2017.04.047](https://doi.org/10.1016/j.nanoen.2017.04.047)
24. J. Cui, P.F. Li, Z.F. Chen, K. Cao, D. Li et al., Phosphor coated NiO-based planar inverted organometallic halide perovskite solar cells with enhanced efficiency and stability. *Appl. Phys. Lett.* **109**(17), 171103 (2016). doi:[10.1063/1.4965838](https://doi.org/10.1063/1.4965838)
25. D. Li, J. Cui, H. Li, D.K. Huang, M.K. Wang, Y. Shen, Graphene oxide modified hole transport layer for $\text{CH}_3\text{NH}_3\text{PbI}_3$ planar heterojunction solar cells. *Sol. Energy* **131**, 176–182 (2016). doi:[10.1016/j.solener.2016.02.049](https://doi.org/10.1016/j.solener.2016.02.049)
26. H. Luo, X.H. Lin, X. Hou, L.K. Pan, S.M. Huang, X.H. Chen, Efficient and air-stable planar perovskite solar cells formed on graphene-oxide-modified PEDOT:PSS hole transport layer. *Nano-Micro Lett.* **9**(4), 39 (2017). doi:[10.1007/s40820-017-0140-x](https://doi.org/10.1007/s40820-017-0140-x)
27. D. Li, J. Cui, H. Zhang, H. Li, M.K. Wang, Y. Shen, Effect of hole transport layer in planar inverted perovskite solar cells. *Chem. Lett.* **45**(1), 89–91 (2016). doi:[10.1246/cl.150888](https://doi.org/10.1246/cl.150888)
28. K.Y. Yan, Z.H. Wei, T.K. Zhang, X.L. Zheng, M.Z. Long et al., Near-infrared photoresponse of one-sided abrupt $\text{MAPbI}_3/\text{TiO}_2$ heterojunction through a tunneling process. *Adv. Funct. Mater.* **26**(46), 8545–8554 (2016). doi:[10.1002/adfm.201602736](https://doi.org/10.1002/adfm.201602736)
29. B.G. Streetman, S.K. Banerjee, *Solid State Electronic Devices* (Prentice Hall, Upper Saddle River, 2006)
30. E.K. Liu, B.S. Zhu, J.S. Luo, *The Physics of Semiconductors* (Publishing House of Electronics Industry, Beijing, 2012)
31. S.D. Stranks, G.E. Eperon, G. Grancini, C. Menelaou, M.J.P. Alcocer, T. Leijtens, L.M. Herz, A. Petrozza, H.J. Snaith, Electron-hole diffusion lengths exceeding 1 micrometer in an organometal trihalide perovskite absorber. *Science* **342**(6156), 341–344 (2013). doi:[10.1126/science.1243982](https://doi.org/10.1126/science.1243982)
32. N. Tripathi, M. Yanagida, Y. Shirai, T. Masuda, L.Y. Han, K. Miyano, Hysteresis-free and highly stable perovskite solar cells produced via a chlorine-mediated interdiffusion method. *J. Mater. Chem. A* **3**(22), 12081–12088 (2015). doi:[10.1039/C5TA01668A](https://doi.org/10.1039/C5TA01668A)
33. E.M. Hutter, G.E. Eperon, S.D. Stranks, T.J. Savenije, Charge carriers in planar and meso-structured organic-inorganic perovskites: mobilities, lifetimes, and concentrations of trap states. *J. Phys. Chem. Lett.* **6**(15), 3082–3090 (2015). doi:[10.1021/acs.jpcclett.5b01361](https://doi.org/10.1021/acs.jpcclett.5b01361)
34. J. Min, Z.G. Zhang, Y. Hou, C.O. Ramirez Quiroz, T. Przybilla et al., Interface engineering of perovskite hybrid solar cells with solution-processed perylene-diimide heterojunctions toward high performance. *Chem. Mater.* **27**(1), 227–234 (2015). doi:[10.1021/cm5037919](https://doi.org/10.1021/cm5037919)
35. E. Edri, S. Kirmayer, M. Kulbak, G. Hodes, D. Cahen, Chloride inclusion and hole transport material doping to improve methyl ammonium lead bromide perovskite-based high open-circuit voltage solar cells. *J. Phys. Chem. Lett.* **5**(3), 429–433 (2014). doi:[10.1021/jz402706q](https://doi.org/10.1021/jz402706q)
36. U. Wurfel, D. Neher, A. Spies, S. Albrecht, Impact of charge transport on current-voltage characteristics and power-conversion efficiency of organic solar cells. *Nat. Commun.* **6**, 6951 (2015). doi:[10.1038/ncomms7951](https://doi.org/10.1038/ncomms7951)
37. S.M. Sze, K.K. Ng, *Physics of Semiconductor Devices* (Wiley, New York, 1981)
38. W.J. Ke, G.J. Fang, J.W. Wan, H. Tao, Q. Liu et al., Efficient hole-blocking layer-free planar halide perovskite thin-film solar cells. *Nat. Commun.* **6**, 6700 (2015). doi:[10.1038/ncomms7700](https://doi.org/10.1038/ncomms7700)
39. J. Dong, J.J. Shi, D.M. Li, Y.H. Luo, Q.B. Meng, Controlling the conduction band offset for highly efficient ZnO nanorods based perovskite solar cell. *Appl. Phys. Lett.* **107**(7), 073507 (2015). doi:[10.1063/1.4929435](https://doi.org/10.1063/1.4929435)
40. J. Qing, H.T. Chandran, Y.H. Cheng, X.K. Liu, H.W. Li, S.W. Tsang, M.F. Lo, C.S. Lee, Chlorine incorporation for enhanced performance of planar perovskite solar cell based on lead acetate precursor. *ACS Appl. Mater. Interface* **7**(41), 23110–23116 (2015). doi:[10.1021/acsami.5b06819](https://doi.org/10.1021/acsami.5b06819)
41. Y.K. Wang, D.Z. Yang, X.K. Zhou, S.M. Alshehri, T. Ahamad, A. Vadim, D.G. Ma, Vapour-assisted multi-functional perovskite thin films for solar cells and photodetectors. *J. Mater. Chem. C* **4**(31), 7415–7419 (2016). doi:[10.1039/C6TC00747C](https://doi.org/10.1039/C6TC00747C)
42. H.Y. Zhang, J.J. Shi, X. Xu, L.F. Zhu, Y.H. Luo, D.M. Li, Q.B. Meng, Mg-doped TiO_2 boosts the efficiency of planar perovskite solar cells to exceed 19%. *J. Mater. Chem. A* **4**(40), 15383–15389 (2016). doi:[10.1039/C6TA06879K](https://doi.org/10.1039/C6TA06879K)
43. J. Chen, J. Xu, L. Xiao, B. Zhang, S.Y. Dai, J.X. Yao, Mixed-organic-cation $(\text{FA})_x(\text{MA})_{1-x}\text{PbI}_3$ planar perovskite solar cells with 16.48% efficiency via a low-pressure vapor-assisted solution process. *ACS Appl. Mater. Interface* **9**(3), 2449–2458 (2017). doi:[10.1021/acsami.6b13410](https://doi.org/10.1021/acsami.6b13410)